Biosensors and Bioelectronics 142 (2019) 111532

Contents lists available at ScienceDirect

Biosensors and Bioelectronics

journal homepage: www.elsevier.com/locate/bios

A novel label-free electrochemical impedance aptasensor for highly sensitive detection of human interferon-gamma based on target-induced exonuclease inhibition

Huan Li, Shihao Song, Meiqi Wen, Ting Bao, Zhen Wu, Huayu Xiong, Xiuhua Zhang, Wei Wen*, Shengfu Wang

Hubei Collaborative Innovation Center for Advanced Organic Chemical Materials, Ministry of Education Key Laboratory for the Synthesis and Application of Organic Functional Molecules & College of Chemistry and Chemical Engineering, Hubei University, Wuhan, 430062, PR China

ARTICLE INFO

Keywords:
Tuberculosis
Human interferon gamma
Electrochemical impedance aptasensor
Target-induced exonuclease inhibition

ABSTRACT

In this paper, a novel label-free electrochemical impedance aptasensor for highly sensitive detection of IFN-γ based on target-induced exonuclease inhibition was constructed. For this purpose, we designed a DNA hairpin modified on the gold electrode whose loop was the aptamer of the IFN-γ, and the stem was 5′-thiol-modified. In the absence of IFN-γ, Exonuclease III (Exo III) and Exonuclease I (Exo I) digested the double-stranded and single-stranded strands of the hairpin DNA, respectively, causing smaller impedance value on the surface of the electrode. In the presence of IFN-γ, the function of Exo III was greatly inhibited by the binding of the aptamer with the target, and it stopped after cutting three bases of the hairpin DNA. Forming a major target-bound aptamer digestion product, it could not be digested by Exo I, so there was larger impedance on the electrode surface. The calibration curve for IFN-γ was linear in the range of 1 pM–50 nM with the detection limit (LOD) of 0.7 pM. The proposed aptasensor proved good selectivity and reproducibility, and low cost. In addition, the biosensor was able to detect IFN-γ in serum samples successfully, which is expected to provide an efficient method for TB diagnosis at early stages.

1. Introduction

Tuberculosis, one of the top ten causes of death in the worldwide, is a lethal chronic disease aroused by *Mycobacterium tuberculosis* (Bloom and Murray, 1992; Telenti et al., 1993). In order to reduce the global health threat by tuberculosis, it is essential to identify potential tuberculosis patients to study the disease. Several recent studies have shown that cytokines associated with tuberculosis can be used as biomarkers to monitor potential tuberculosis (Abnous et al., 2017; Wallis et al., 2009). Among them, interferon-gamma (IFN-γ), a member of the cytokine family, is a 15.5 KDa glycoprotein molecule was studied as a potential biomarker. Produced by activated T cells and natural killer cells (NK cells), IFN-γ possesses biologically antiviral, immunomodulatory, and antitumor properties (Farid et al., 2015; Zaidi and Merlino, 2011; Bao et al., 2019). In the early stages of *Mycobacterium tuberculosis* infection, as IFN-γ is highly expressed (Itoh et al., 1998) and extremely low level (within pM range) in the body, it has received widespread attention as a marker of tuberculosis (Ma et al., 2018). Therefore, it is urgent for us to take active and effective measures to detect and quantify IFN-γ. Currently, there is increasingly number of methods available to determine IFN-γ, such as enzyme-linked immunosorbent assay (ELISA) (Josephine et al., 2006), colorimetic (Zhou et al., 2012), fluorescent detection (Dhenadhayalan et al., 2018), interferon gamma releasing assay (IGRA) (Lee et al., 2019) and electrochemical analysis methods (Liu et al., 2010, 2011). Thereinto, electrochemical analysis methods have been effective in analytical testing and gradually become a powerful tool due to their low cost, rapid response, and high sensitivity. So, it is quite necessary to construct an electrochemical sensing platform with high sensitivity and selectivity to detect IFN-γ.

The aptamer is a small fragment of the oligonucleotide sequence obtained by *in vitro* screening, which has the characteristics of simple chemical synthesis and modification, easy mass production, and better stability (Tuerk and Gold, 1990). In the meantime, aptamers have a clear three-dimensional structure, enabling them to bind to the corresponding ligand with higher affinity and selectivity (Willner and Zayats, 2007; Mayer, 2009). In recent years, combined with the excellent performance and accuracy of electrochemical methods,

* Corresponding author.
E-mail address: wenwei@hubu.edu.cn (W. Wen).

https://doi.org/10.1016/j.bios.2019.111532
Received 23 May 2019; Received in revised form 19 July 2019; Accepted 22 July 2019
Available online 25 July 2019
0956-5663/

electrochemical aptasensors have been widely reported. Usually, electrochemical aptasensors include two forms: label-free and label-based detection. Among them, label-based electrochemical aptasensors are reported in large proportion. The representative cases are intramolecular conformational changes (Zuo et al., 2007; Su et al., 2016) and target-induced strand displacement (Xiao et al., 2005; Cui et al., 2013). Despite the rapid advanced development of labeled electrochemical aptasensor, still there are several limitations: First, only a few aptamers have inward structure-switching functionality, and target-binding site must be recognized before the complicated design for going through a large target-induced conformational change (Wang et al., 2018; Zheng et al., 2012; Xu et al., 2014; Yu et al., 2017). Then, since aptamers usually have excellent affinity for the complementary DNA and a relatively weaker binding to the target small molecule in the strand displacement strategies, the sensitivity of the aptasensor and its application area are restricted (Canoura et al., 2018). In addition, aptasensors based on electrochemical beacons (e.g., ferrocene or methylene blue) and nanomaterials (e.g., gold nanoparticles, multi-walled carbon nanotubes and so forth) are complicated, costly, and labor intensive (Xia et al., 2015; Song et al., 2019; Ardakani et al., 2018). Thus, there is an urgent need to develop label-free electrochemical aptasensors for sensitive, easy to operate and cost-effective analytical detection.

Label-free electrochemical aptasensors mainly measure ligand-aptamer interactions through electrochemical impedance recording the change of the electron transfer impedance between the cation or anion redox probe ($[Ru(NH_3)_6]^{3+}$ or $[Fe(CN)_6]^{3-/4-}$) and the conducting electrode site in the solution (Munoz et al., 2017; Hianik and Wang, 2009). Although it does not require expensive reagents or labels (Golichenari et al., 2018; Hu et al., 2018), it is not satisfactory enough for sensitivity and innovation, rendering label-free electrochemical aptasensors relatively few reports. The concept, target-induced exonuclease inhibition, was first proposed by Xiao's group (Wang et al., 2018). They discovered that target binding could greatly inhibited exonuclease III (Exo III)-mediated digestion of combination of small molecule and aptamer. Specifically, Exo III stopped the digestion of four bases before the target and aptamer binding regions. Although they achieved a big breakthrough in the field of aptamer research, their research objects were limited to small molecules, and the main source of detection technology was fluorescence (Canoura et al., 2018). More importantly, combined with label-free electrochemical aptasensors, target binding aptamer-induced exonuclease inhibition may be a new thought for detecting macromolecules and it has not been reported yet. Inspired by the above outcome, we try to come up with a label-free electrochemical aptasensor based on target-induced exonuclease inhibition for detection of IFN-γ, with the aim to improve the sensitivity of label-free aptasensor, as well as to explore target binding-induced exonuclease inhibition for macromolecule detection.

In this work, we utilized aptamer as biomolecular recognition element and redox couple $[Fe(CN)_6]^{3-/4-}$ as signal probe for highly sensitive detection of IFN-γ based on target-induced exonuclease inhibition. The 5′-thiol-modified hairpin DNA (we were all referred to aptamer below) was assembled on the surface of the gold electrode at room temperature overnight, followed by blocking with MCH to eliminate non-specific adsorption of the electrode surface. Then the electrode was cultured in a mixed solution of exonuclease III (Exo III) and exonuclease I (Exo I). In the absence of target, the aptamer was sequentially cleaved into short chain products by dual-exonuclease, so that the electron transfer resistance (R_{et}) of the signal probe was relatively small, regarded as R_{et0}. Upon addition of target, the binding of the target to the aptamer affected the shearing of Exo III, which exactly stopped digesting four bases before the target binding region, forming the major target-bound aptamer digestion products (Canoura et al., 2018), causing lager impedance in the system, expressed as R_{et}. The variation of the relative impedance ($\Delta R = R_{et} - R_{et0}$) was used to evaluate the concentration of the IFN-γ immobilized on the electrode. Based on these mechanisms, we proposed a label-free electrochemical impedance aptasensor with fast response, simple operation and low cost for determination of IFN-γ based on target-induced exonuclease inhibition.

2. Experimental section

2.1. Chemicals and reagents

Exonuclease I (20 units μL^{-1}) and Exonuclease III (200 units μL^{-1}) were purchased from Thermo Fisher Scientific (USA). Potassium ferricyanide ($K_3[Fe(CN_6)]$), potassium ferrocyanide ($K_4[Fe(CN_6)]$), 20 mM Tris-HCl (composed of 100 mM NaCl and 5 mM $MgCl_2$, pH = 7.4, which was acted as the buffer solution for the oligonucleotide stock solutions) and bovine serum albumin (BSA) were all obtained from Aladdin Bio-Chem Technology Co., Ltd. (Shanghai, China), Thrombin (Tb), myoglobin (Mb), 6-mercapto-1-hexanol (MCH) and phosphate buffer solution (20 × PBS buffer, pH = 7.4 to 7.6) were all attained from Sigma Aldrich (USA). Human IFN-γ ELISA Kit was received from Sangon Biotech Co., Ltd. (Shanghai, China). And the oligonucleotide with the sequence of: 5′–SH–$(CH_2)_6$- GGTCTCAGTCAG***GGGGTTGGTTGTGTTGGGTGTTGTGT***CTGACTG-3' (The bold italicized part was the aptamer sequence formed loop-structure of the hairpin DNA) was synthesized and purified. The whole reagents mentioned above were of analytical grade or higher and would not be required any deliberate purification before used. Deionized water was purified to a resistance of 18.25 MΩ cm.

2.2. Instrumentation

PSH-500A biochemical incubator, medical centrifuge, constant temperature water bath, and vortex were essential instruments for electrochemical analysis. The data of the cyclic voltammetry (CV) curve and the electrochemical impedance spectroscopy (EIS) curve were all collected by CHI 660E electrochemical workstation (CH Ins., Shanghai, China), which were the main technology of this experiment. Electrochemical detection followed the three-electrode system: Gold electrode (GE, Ø = 2 mm), calomel electrode, platinum electrode in turn as working electrode, reference electrode and auxiliary electrode.

2.3. Treatment of GE prior to use

The situation was usually like this, eight identical gold electrodes were used as a set of experiments. After polishing on the suede with 0.05 μm alumina polishing powder for 10 min, the electrodes were sequentially ultrasonic cleaning in water, ethanol and water, 5 min at a time interval in order to remove impurities adsorbed on the electrode surface, and finally, an electrochemical cleaning process was performed, which were activated in 0.5 M H_2SO_4 with scan range from −0.3 V to 1.5 V and a scan rate of 0.1 V s^{-1}.

2.4. Preparation of label-free electrochemical aptasensor

The assembly of the aptamer was the first step. Firstly, in order to get a stem-loop DNA structure, the aptamer (A total of 240 μL, the final concentration was 10 μM) was heated to 95 °C in water bath and held for 5 min, then slowly lowered to room temperature and placed at −4 °C for subsequent use (Huang et al., 2017). The well-prepared GE was immersed in the 50 μL aptamer (0.5 μM), diluted by 20 mM tris-HCl, at room temperature for 12 h. Secondly, the position without aptamer was blocked with MCH (1 mM) for 1 h to prevent non-specific adsorption. Thirdly, the GE was soaked in 50 μL of different concentrations of IFN-γ dissolved with PBS (pH = 7.4) in the biochemical incubator at 37 °C for 2 h. Finally, the GE was modified in a soaking manner with a mixture of 20 μL Exo I (0.2 U μL^{-1}) and 20 μL Exo III (0.1 U μL^{-1}) for 2 h. After each step, the GE was carefully washed with ultrapure water.

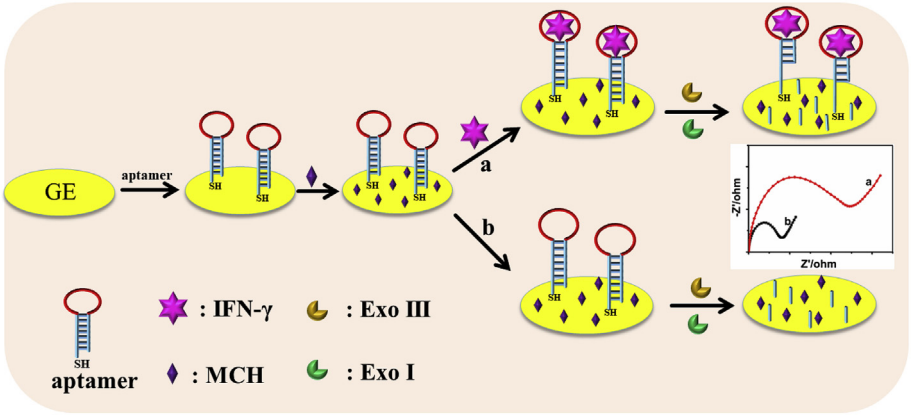

Scheme 1. Schematic illustration of designed electrochemical impedance aptasensor for detection of IFN-γ.

2.5. Electrochemical impedance detection

0.5 mM $K_3[Fe(CN)_6]/K_4[Fe(CN)_6]$ (1:1), including 0.5 M KCl was put on an electrochemical cell, and then three-electrode system was constructed. All electrochemical impedance measurements were implemented by measuring the surface electron transfer of the electrode with or without target, which were collected as a form of Nyquist plots (Min et al., 2008). Furthermore, a scanning frequency ranged from 0.01 to 10^5 Hz, while its amplitude was 0.05.

3. Results and discussion

3.1. Principle discussion and feasibility for detecting IFN-γ

The electrochemical impedance aptasensor was built on account of specific recognition of aptamer and IFN-γ, inhibition of their conjugates against Exo III cleavage, and co-modulation of Exo I and Exo III. As shown in Scheme 1, the aptamer was self-assembled on the polished GE by Au–S bond and reacted for 12 h at room temperature. Then, 1 mM MCH was used to block unligated sites and prevented non-specific adsorption for 1 h. After that, a certain concentration of IFN-γ was combined with the aptamer, which greatly inhibited the activity of the Exo III in the mixed solution of the Exo III and the Exo I. Exo III catalyzed the 3′-blunt end of double-stranded structure of aptamer stem to gradually remove three bases before the target-binding domain (Canoura et al., 2018), and the remaining double-stranded structure could not be digested by the Exo I in the solution, leading to larger impedance due to more such structures. In this situation, the electron transfer resistance referred to as R_{et}. Conversely, in the absence of the IFN-γ, the double-stranded structure of aptamer stem was totally decomposed by Exo III and the remaining single-stranded structure was successfully digested by Exo I, so the hindrance of the electrode surface was relatively reduced, which was referred to as R_{et0}. In both cases, the difference in electron transfer resistance was considered to be ΔR, ($\Delta R = R_{et} - R_{et0}$), which was also conducted as the signal output for us to establish the relationship between the concentration of IFN-γ and their EIS responses.

We assumed when the electrode was blocked by MCH, the electron transfer resistance on the surface of the electrode got significantly increased. After culturing IFN-γ at various concentrations, the impedance was further increased. Subsequently, the Exo III and the Exo I were cultured, with the concentration of IFN-γ increased, the digestion of the Exo III to the double-stranded part of the aptamer was significantly inhibited, and the electron transfer resistance was greater. In contrast, when the target concentration was smaller or even absent, the shearing of the double strand by the Exo III and the shearing of the single strand by the Exo I caused the electron transfer resistance to become smaller. In Fig. 1A, curve a, curve b and curve c, the concentrations of IFN-γ at 0 nM, 0.01 nM and 50 nM successively, the impedance values were shown. In addition, the curve d was the impedance plots after the electrode was blocked by MCH. It was not difficult to find that the resistance of 50 nM was significantly larger than the other two values, which was consistent with our previous assumption. In Fig. 1B, the circuit diagram was used to simulate the resistance, among which R_{et} corresponded to the diameter of the semicircle in the Nyquist plot (Zhao et al., 2019) and was unified as the impedance response we got each time.

3.2. The characterization of CV and EIS for each step of electrode modification

To better characterize the electrode surface, CV and EIS were used to display the modification condition of each layer on the GE. As shown in Fig. 2A, the larger the redox current, the better the conductivity of the electrode interface (Wang et al., 2017). For instance, in curve a, a reversible cyclic voltammogram was obtained for bare GE, with the maximum redox current, which indicated the electrode surface was the most conductive at this time. Hereafter, GE was modified with aptamer (curve b), IFN-γ (curve d) and dual-exonuclease (curve e) in 0.5 mM $[Fe(CN)_6]^{3-/4-}$ in the voltage range between −0.2 to 0.6 V with a scanning rate of 0.1 V s^{-1}. We could clearly see that from curve a to curve d, the redox current was getting smaller and smaller, and the conductivity of the electrode surface was getting worse. This may be owing to the negatively charged phosphate backbone of the aptamer had electrostatic repulsion to the $[Fe(CN)_6]^{3-/4-}$ probe. Intriguingly, when the GE was reacted in the double-exonuclease mixed solution, the resistance to the transmission of electron was not as serious as the previous process due to the partial shear of the Exo III to the stem of the aptamer, which exactly reflected in curve e, a slight increase in redox peaks.

The situation mentioned above was consistent with the EIS in Fig. 2B, only when the redox peak increased, the resistance was reduced. And the diameter of the semicircle in EIS was equal to the value of R_{et}. In curve a, the better conductivity of the bare electrode presents a negligible impedance, showing a straight line in the EIS. As the aptamer (curve b) and MCH (curve c) were modified on the GE, the R_{et} raised significantly, 20.78 KΩ and 46.97 KΩ respectively. Furthermore, when the electron was modified with 2 nM IFN-γ (curve d), the R_{et} increased dramatically to 58.64 KΩ, whose reason for this phenomenon was explained in the above analysis of cyclic voltammetry. Finally, the GE was treated with double-exonuclease mixed solution (curve e), the R_{et} abruptly decreased to 40.50 KΩ. Although the integrating of the target to the aptamer greatly inhibited the digestion of the Exo III, the Exo III still functioned to cleave three bases of the aptamer. That was enough to get the electron transfer on the electrode surface reduced. As shown above, good performance of CV and EIS indicated that every step of the modification was successfully as we expected.

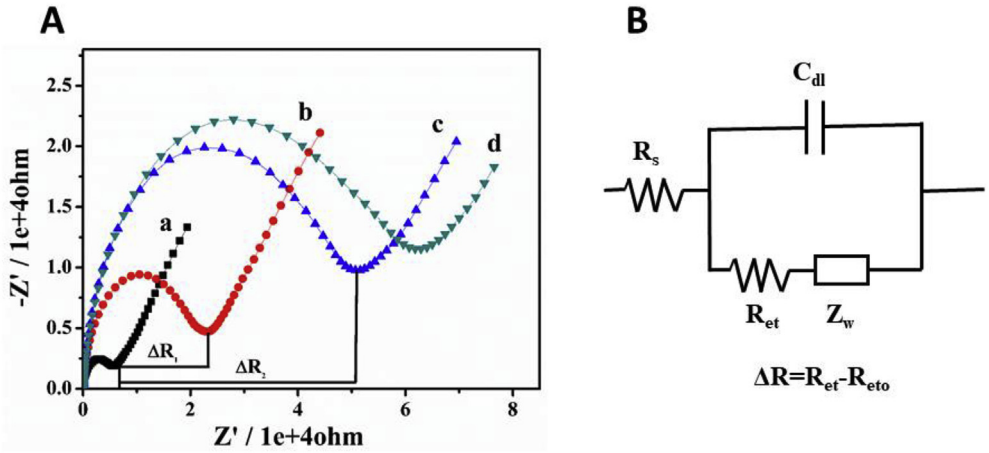

Fig. 1. (A) Nyquist plots of the biosensor corresponding to different concentrations of target: (a) 0 nM; (b) 0.01 nM; (c) 50 nM; and (d) The GE was blocked by MCH; (B) Equivalent circuit of electrochemical impedance spectroscopy.

3.3. The optimization of experimental conditions

In order to get an optimized experimental state, it was quite necessary to optimize some important aspects of the experiment, the assembly time of aptamer, the concentration of the aptamer, the concentration ratio of the two exonucleases, and the reaction time of target were what we explored. In all optimization experiments, we chose the IFN-γ concentration of 2 nM as the control condition.

First of all, we optimized the assembly time of aptamer. As shown in Fig. 3A, the time which the aptamer modified on the electrode by the Au–S bond was studied from 3 h to 15 h. It was not difficult to see that the impedance signal was rapidly increasing from 3 h to 12 h, and it reached a platform at 12 h. With the increasing assembly time, the more aptamers were attached to the GE, bringing out more target-induced exonuclease inhibition process and lager impedance signal. So 12 h was selected as the optimum time to assemble the aptamer. Next, as shown in Fig. 3B, the impedance signal changed as the aptamer concentrations increased from 0.1 to 0.7 μM were investigated. When it reached to 0.5 μM, its signal reached maximum and then slowly began to decrease, which was mainly because of the area of the electrode being limited, and the superfluous aptamer was neither connected to the electrode surface nor connected to more IFN-γ, but increased the burden of electron transfer. Therefore, 0.5 μM aptamer was selected for the next study.

Then, the concentration ratio of Exo I and Exo III was also explored. The number of aptamers and double-exonuclease attached to the electrodes should be suitable. If the Exo III was excessive, it would not be able to shear specific number of aptamers, which caused a larger background signal, while the Exo III was insufficient (the Exo I was excessive), the adding of IFN-γ did not cause a large signal fluctuation, leading to narrow detection range. As presented in Fig. 3C, the concentration ratio of Exo I and Exo III was investigated from 1:1 to 6:1, which obviously displayed highest signal when the ratio was 2:1 and the maximum response was obtained, thus 2:1 was the most suitable condition for the experiment. The reaction time of IFN-γ with aptamer was also crucial to the experiment, as it directly influenced the process of the target-induced exonuclease inhibition. So, we continued to optimize the reaction time of IFN-γ with aptamer. As seen in Fig. 3D, the impedance signal augmented with the extension of culture time of target until it reached a platform at 105 min. Hence, 105 min was chose as the best reaction time of IFN-γ with aptamer.

3.4. Analytical application

Different concentrations of the IFN-γ presented in Fig. 4 were to investigate the performance of this aptasensor. The EIS responses of the aptasensor were investigated in Fig. 4A, which revealed as the concentration of IFN-γ increased, the EIS response signal and Δ*R* value increased as well. Fig. 4B plotted the variation of impedance value (Δ*R*) and the concentration of IFN-γ, Δ*R* shown good linear relation with the logarithm of IFN-γ concentration ranging from 1 pM to 50 nM. The regression equation was described as follows: $\Delta R = 8296.6 \lg C + 8545.8$ ($R^2 = 0.9975$). The detection limit for IFN-γ was obtained to be 0.7 pM (signal-to-noise was 3). Compared with other reports of

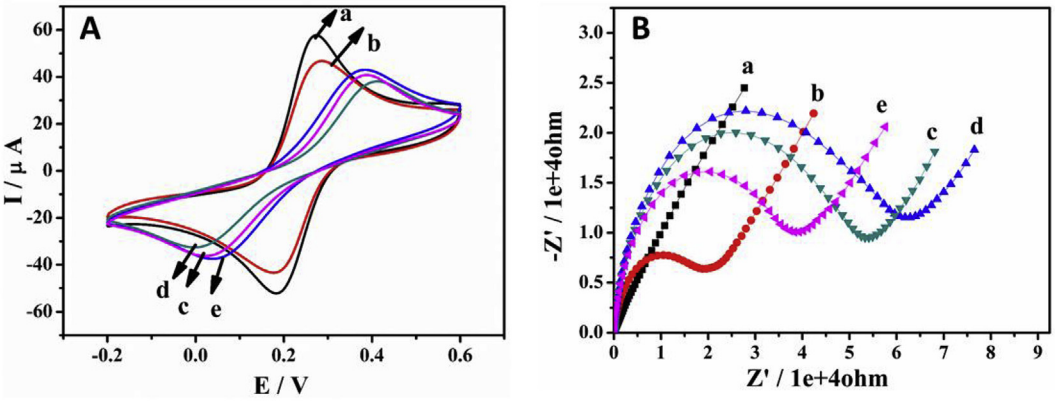

Fig. 2. (A) Cyclic voltammograms and (B) Nyquist plots of the biosensor: (a) bare GE; (b) aptamer/GE; (c) MCH/aptamer/GE; (d) 2 nM IFN-γ/MCH/aptamer/GE; (e) dual-exonuclease/2 nM IFN-γ/MCH/aptamer/GE.

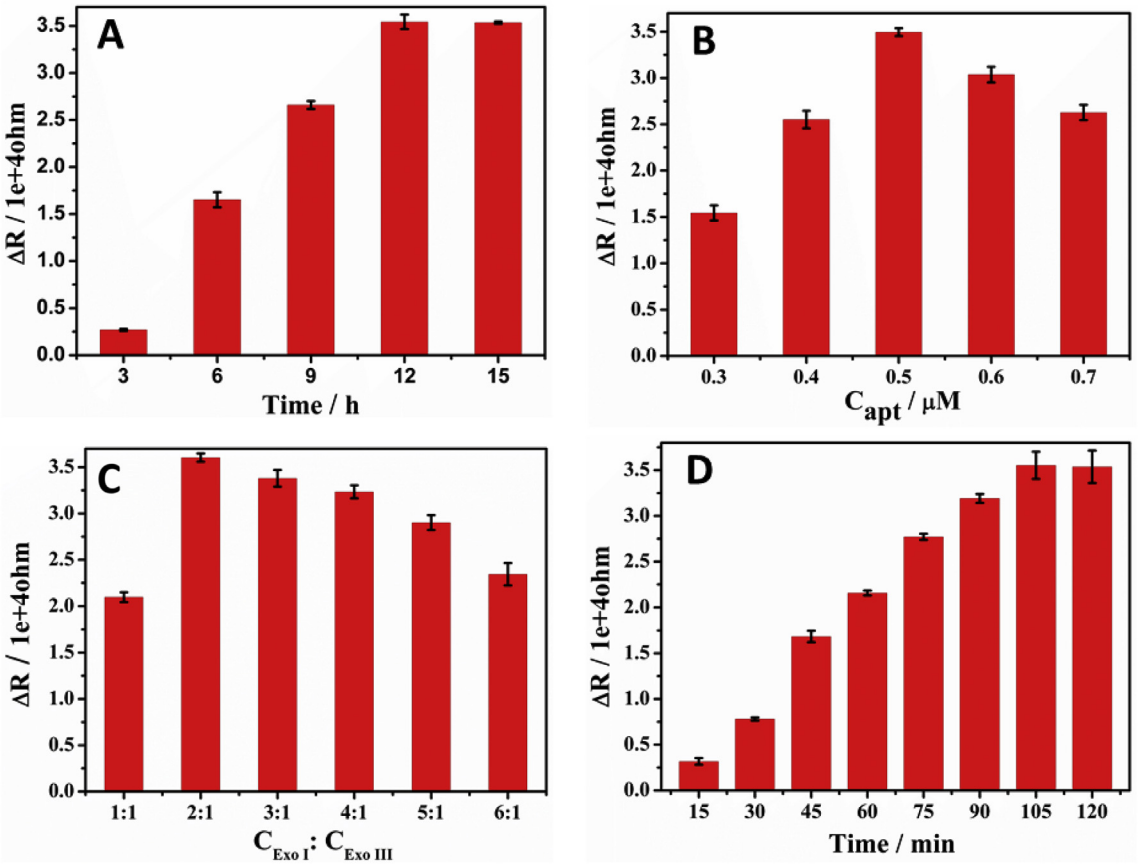

Fig. 3. Optimization of experimental conditions of (A) The incubation time of aptamer; (B)The concentration of aptamer; (C) The concentration ratio of Exo I and Exo III; (D) The reaction time of IFN-γ and aptamer.

detecting the IFN-γ shown in Table S1 in the Supporting Information, the aptasensor we designed with a wider detection range and lower detection limit. That was mainly due to the rapid response, sensitive characteristics of the electrochemical impedance aptasensor, the excellent catalytic function of Exo I and Exo III, and superior performance of target binding aptamer-induced exonuclease inhibition.

3.5. The reproducibility and selectivity of the designed aptasensor

The reproducibility of the aptasensor was displayed in Fig. 5A, detected by using six electrodes to investigate the same concentration of IFN-γ (2 nM) under the identical conditions. The relative standard deviation (RSD) of the average value was calculated to be 1.43%. In the meantime, the same electrode was picked to verify reproducibility for six times in Fig. 5B with 2 nM IFN-γ, the RSD was only 0.93%, excellent reproducibility also reflected the great advantages of this aptasensor that we had established.

To further discuss the performance of our aptasensor, we had carried out this scheme on the analog of the IFN-γ (BSA, Tb, and Mb) under the same conditions. In Fig. 5C, it showed the different EIS responses of this biosensor after the introduced of a blank sample (PBS, pH = 7.4), 5 nM of IFN-γ, 100 nM of BSA, 100 nM of Tb, 100 nM of Mb. A tiny EIS response was obtained when the aptasensor was tested with several possible interfering substances at the concentration were even 20 times

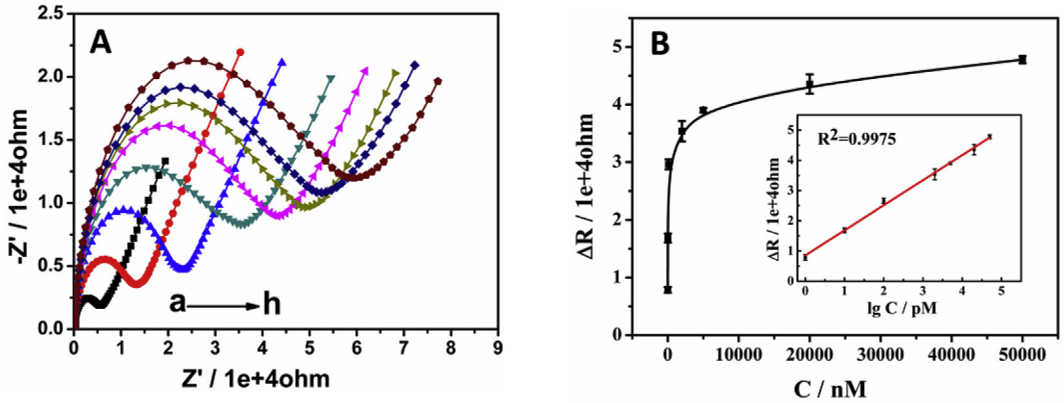

Fig. 4. (A) EIS responses corresponding to different concentrations of IFN-γ: (a) 0, (b) 1 pM, (c) 10 pM, (d) 0.1 nM, (e) 2 nM, (f) 5 nM, (g) 20 nM, (h) 50 nM. (B) Linear relationship between EIS responses and the logarithm concentration of IFN-γ ranging from 1 pM to 20 nM.

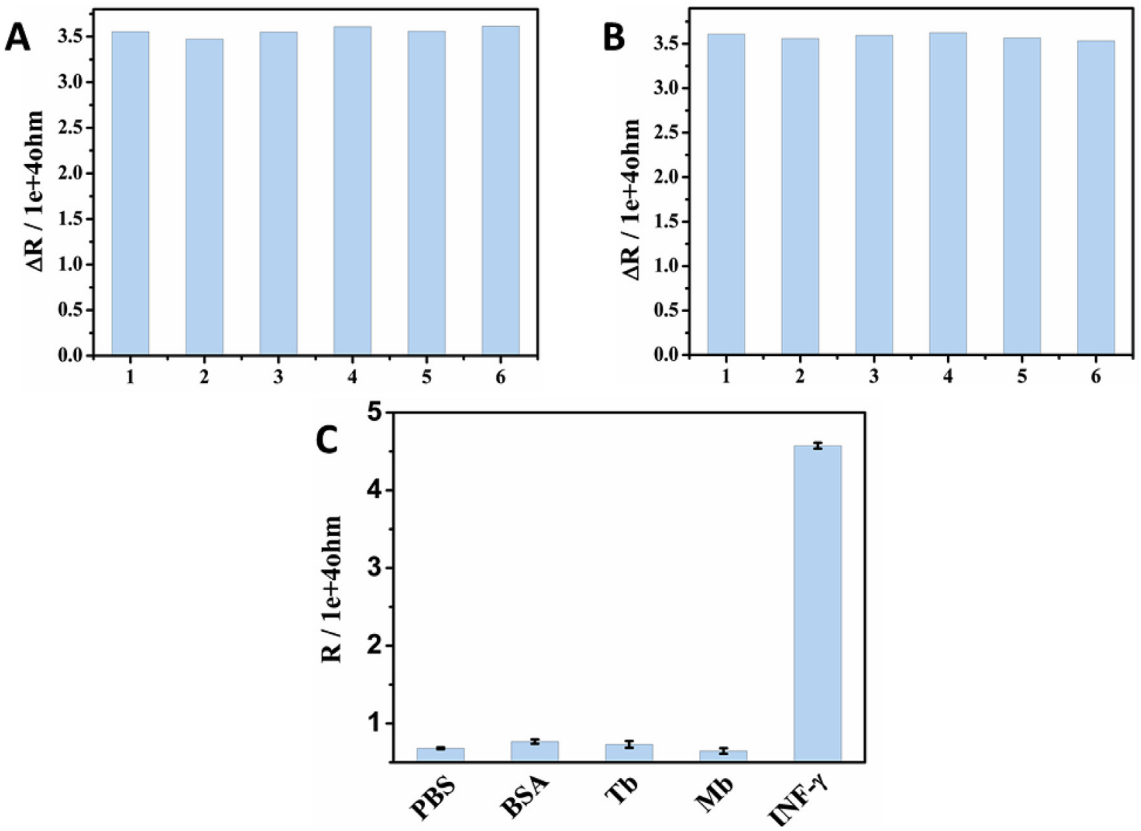

Fig. 5. Repeatability experiment of the biosensor under the optimized condition; (A) with six different electrodes; (B) the same electrode was evaluated for six times; (C) specificity of the biosensor for IFN-γ detection.

that of the IFN-γ. In contrast, when the aptasensor only added 5 nM IFN-γ, large impedance response was achieved, which could be ascribed to the specific binding between the IFN-γ and its aptamer. From this we could easily see that, the aptasensor had satisfactory selectivity and nice reproducibility.

3.6. The testing of serum sample

In order to further evaluate the applicability of this aptasensor, different concentrations of IFN-γ were adding to normal human serum which was diluted 100-fold for spiked recovery experiment. The proposed aptasensor and the commercial ELISA method (Liu et al., 2015) were used in three groups of identical serum samples to detect IFN-γ. As shown in Table S2 in the Supporting Information, when various concentrations of the IFN-γ (2 pM, 10 pM, and 15 pM) were added to the serum sample, the recoveries detected by the aptasensor were ranging from 91.83% to 101.90%, with an RSD of less than 6.5%, and the recoveries detected by the commercial ELISA method were ranging from 94.54% to 98.35%, with an RSD of less than 5%. In the meantime, the relative difference less than 6.38% suggested that the aptasensor we built had an acceptable accuracy in the detection of IFN-γ in complex biological samples, and it was expected for clinical testing.

4. Conclusion

In summary, we had successfully developed a label-free electrochemical aptasensor based on target-induced exonuclease inhibition for highly sensitive detection of IFN-γ. First, the specific binding of the target to the aptamer allowed this aptasensor to have a nice selectivity; Second, the aptamer bound with the IFN-γ affected the function of the Exo III, whose catalysis activity was stopped after cutting three bases of the aptamer, causing large impedance on the electrode surface. Thus, the impedance response increased with the addition of IFN-γ mediated by double-exonuclease. Third, the strategy target-induced exonuclease inhibition combined with electrochemical impedance aptasensor was for the first time in the detection of macromolecules (IFN-γ). In addition to the above three outstanding merits, the highly sensitive aptasensor which we designed to detected IFN-γ had the advantages of simple operation, cost effective and with a low detection limit of 0.7 pM. Simultaneously, it showed good performance in serum samples. In a word, the aptasensor described above would be a good platform for clinical diagnosis of latent TB with attractive prospects, and the strategy used in this work was expected to further study different label-free electrochemical aptasensor for the detection of other biomolecules.

Declaration of competing interest

The authors declare that they have no known competing financial interests or personal relationships that could have appeared to influence the work reported in this paper.

CRediT authorship contribution statement

Huan Li: Writing - original draft, Formal analysis. **Shihao Song:** Writing - original draft, Formal analysis. **Meiqi Wen:** Formal analysis. **Ting Bao:** Formal analysis. **Zhen Wu:** Formal analysis. **Huayu Xiong:** Formal analysis. **Xiuhua Zhang:** Writing - review & editing. **Wei Wen:** Funding acquisition, Investigation, Methodology, Project administration. **Shengfu Wang:** Investigation, Methodology, Project administration.

Acknowledgements

This work was partly financially supported by the National Natural

Science Foundation of China (Nos.21405035) and the General Project Program of the Natural Science Foundation of Hubei Province (No. 2017CFB529).

Appendix A. Supplementary data

Supplementary data to this article can be found online at https://doi.org/10.1016/j.bios.2019.111532.

References

Abnous, K., Danesh, N.M., Ramezani, M., Alibolandi1, M., Hassanabad, K.Y., Bahreyni, A.S.E.A., Taghdisi, S.M., 2017. Microchim Acta 184, 4151–4157.
Ardakani, M.M., Ardakani, Z.T., Sahraei, N., Moshtaghioun, S.M., 2018. Biosens. Bioelectron. 129, 1–6.
Bao, T., Wen, M.Q., Wen, W., Zhang, X.H., Wang, S.F., 2019. Sens. Actuators B Chem. 296, 126606.
Bloom, B.R., Murray, C.J., 1992. Science 257, 1055–1064.
Canoura, J., Wang, Z.W., Yu, H.X., Alkhamis, O., Fu, F.F., Xiao, Y., 2018. J. Am. Chem. Soc. 140 (31), 9961–9971.
Cui, H.F., Fan, H., Lin, Y., 2013. Adv. Mater. Res. 753–755, 2113–2116.
Dhenadhayalan, N., Sriram, M.I., Lin, K.C., 2018. Sens. Actuators B Chem. 258, 929–936.
Farid, S., Choi, X.M.M., Mukherjee, S., Lan, Y., Parikh, D., Poduri, S., Baterdene, U., Huang, C.E., Wang, Y.Y., Burke, P., Dutta, M., Stroscio, Michael A., 2015. Biosens. Bioelectron. 71, 294–299.
Golichenari, B., Velonia, K., Nosrati, R., Nezami, A., Farokhi-Fard, A., Abnous, K., Behravan, J., Aristidis, M., Tsatsakis, 2018. Biosens. Bioelectron. 124–135.
Hianik, T., Wang, J., 2009. Angew. Chem. Int. Ed. 21 (11), 1223–1235.
Hu, X.B.K., Goud b, B., Kumar, V.S., Catanante, G., Li, Z.H., Zhu, Z.J., Marty, J.L., 2018. Sens. Actuators B Chem. 268, 278–286.
Huang, J.Y., Zhao, L., Lei, W., Wen, W., Wang, Y.J., Bao, T., Xiong, H.Y., Zhang, X.Y., Wang, S.F., 2017. Biosens. Bioelectron. 99, 28–33.
Itoh, M., Yano, A., Xie, Q., Iwahashi, K., Takeuchi, Y., Meroni, P.L., Nicoletti, F., 1998. Clin. Exp. Immunol. 111 (3), 513–520.
Josephine, H., Cox, Ferrari, G., Janetzki, S., 2006. Methods 38, 274–282.
Lee, H., Koo, G.W., Min, J.H., Park, T.S., Park, D.W., Moon, J.Y., Kim, S.H., Kim, T.H., Yoon, H.J., Sohn, J.W., 2019. Sci. Rep. 9, 1.
Liu, C., Xiang, G.M., Jiang, D.N., Liu, L.L., Liu, F., Luo, F.K., Pu, X.Y., 2015. Analyst 140.
Liu, Y., Tuleouva, N., Ramanculov, E., Revzin, A., 2010. Anal. Chem. 82, 8131–8136.
Liu, Y., Yan, J., Howland, Michael C., Kwa, T., Revzin, A., 2011. Anal. Chem. 83, 8286–8292.
Ma, K., Zhang, F.L., Sayyadi, Nima, Chen, W.J., Ayad, G., Anwer Care, A., Xu, B., Tian, W.J., Goldys, Ewa M., Liu, G.Z., 2018. ACS Sens. 18, 2313–2317.
Mayer, G., 2009. Angew. Chem. Int. Ed. 48 (15), 2672–2689.
Min, K., Cho, M., Han, S.Y., Shim, Y.B., Ku, J., Ban, C., 2008. Biosens. Bioelectron. 23, 1819–1824.
Munoz, J., Montes, R., Baeza, M., 2017. Trends Anal. Chem. 97, 201–215.
Song, J., Li, S.L., Gao, F., Wang, Q.X., Lin, Z.Y., 2019. Chem. Commun. (J. Chem. Soc. Sect. D) 55, 905.
Su, S., Sun, H.F., Cao, W.F., Chao, J., Peng, H.Z., Zuo, X.L., Yu, L.H., Fan, C.H., Wang, L.H., 2016. ACS Appl. Mater. Interfaces 8 (11), 6826–6833.
Telenti, A., Imboden, P., Marchesi, F., Lowrie, D., Cole, S., Colston, M.J., Matter, L., Schopfer, K., Bodmer, T., 1993. The Lancet 341, 647–650.
Tuerk, C., Gold, L., 1990. Science 249, 505–510.
Wallis, R.S., Doherty, T.M., Onyebujoh, P., Vahedi, M., Laang, H., Olesen, O., Zumla, A., 2009. Lancet Infect. Dis. 9, 162–172.
Wang, Y.J., Zhang, X.Y., Zhao, L., Bao, T., Wen, W., Zhang, X.H., Wang, S.F., 2017. Biosens. Bioelectron. 98, 386–391.
Wang, Z.W., Yu, H.X., Canoura, J., Liu, Y.Z., Alkhamis, O., Fu, F.F., Xiao, Y., 2018. Nucleic Acids Res. 46 (13), gky305.
Willner, I., Zayats, M., 2007. Angew. Chem. Int. Ed. 46, 6408–6418.
Xu, Y.Y., Xu, J., Xiang, Y., Yuan, R., Chai, Y.Q., 2014. Biosens. Bioelectron. 51, 293–296.
Xiao, Y., Piorek, B.D., Plaxco, K.W., Heeger, A.J., 2005. J. Am. Chem. Soc. 127, 17990–17991.
Xia, J.F., Song, D., Wang, Z.H., Zhang, F.F., Yang, M., Gui, R.J., Xia, L., Bi, S., Xia, Y.Z., Li, Y.H., Xia, L.H., 2015. Biosens. Bioelectron. 68, 55–61.
Yu, H.X., Canoura, J., Guntupalli, B., Loub, X.H., Xiao, Y., 2017. Chem. Sci. 8, 131–141.
Zaidi, M.R., Merlino, G., 2011. Clin. Cancer Res. 17 (19), 6118–6125.
Zhao, J.C., Shu, D., Ma, Z.F., 2019. Biosens. Bioelectron. 127, 161–166.
Zheng, D.M., Zou, R.X., Lou, X.H., 2012. Anal. Chem. 84, 3554–3560.
Zhou, W.J., Gong, X., Xiang, Y., Yuan, R., Chai, Y.Q., 2012. Anal. Chem. 86, 953–958.
Zuo, X.L., Song, S.,P., Zhang, J., Pan, D., Wang, L.H., Fan, C.H., 2007. J. Am. Chem. Soc. 129, 1042–1043.